Redox Biology 38 (2021) 101790

Contents lists available at ScienceDirect

Redox Biology

journal homepage: www.elsevier.com/locate/redox

Research Paper

Skin protective and regenerative effects of RM191A, a novel superoxide dismutase mimetic

Artur Shariev [a,d], Spiro Menounos [b], Alistair J. Laos [c], Pooja Laxman [c], Donna Lai [d], Sheng Hua [d], Anna Zinger [e], Christopher R. McRae [f], Llewellyn S. Casbolt [g], Valery Combes [h], Greg Smith [i], Tzong-tyng Hung [j], Katie M. Dixon [a,d], Pall Thordarson [c], Rebecca S. Mason [d,k], Abhirup Das [b,*]

[a] Department of Anatomy and Histology, School of Medical Sciences, University of Sydney, Australia
[b] St. George and Sutherland Clinical School, University of New South Wales, Sydney, Australia
[c] School of Chemistry, The Australian Centre for Nanomedicine and the ARC Centre of Excellence in Convergent Bio-Nano Science and Technology, University of New South Wales, Sydney, Australia
[d] Bosch Institute, Faculty of Medicine and Health, University of Sydney, Australia
[e] Department of Pathology, Faculty of Medicine and Health, University of Sydney, Australia
[f] Department of Chemistry and Biomolecular Sciences, Macquarie University, Sydney, Australia
[g] Department of Biomedical Sciences, Faculty of Medicine and Health Sciences, Macquarie University, Sydney, Australia
[h] School of Life Sciences, University of Technology, Sydney, Australia
[i] School of Medical Sciences, University of New South Wales, Sydney, Australia
[j] Biological Resources Imaging Laboratory, University of New South Wales, Sydney, Australia
[k] Department of Physiology, School of Medical Sciences, University of Sydney, Australia

ARTICLE INFO

Keywords:
SOD mimetic
Anti-inflammatory
UV protection
Immunomodulation
Skin regeneration
Geroprotection

ABSTRACT

Superoxide dismutase (SOD) is known to be protective against oxidative stress-mediated skin dysfunction. Here we explore the potential therapeutic activities of RM191A, a novel SOD mimetic, on skin. RM191A is a water-soluble dimeric copper (Cu^{2+}-Cu^{3+})-centred polyglycine coordination complex. It displays 10-fold higher superoxide quenching activity compared to SOD as well as significant antioxidant, anti-inflammatory and immunomodulatory activities through beneficial modulation of several significant inflammatory cytokines *in vitro* and *in vivo*.

We tested the therapeutic potential of RM191A in a topical gel using a human skin explant model and observed that it significantly inhibits UV-induced DNA damage in the epidermis and dermis, including cyclobutane pyrimidine dimers (CPD), 8-oxo-guanine (8-oxoG) and 8-nitroguanine (8NGO). RM191A topical gel is found to be non-toxic, non-teratogenic and readily distributed in the body of mice. Moreover, it significantly accelerates excisional wound healing, reduces 12-O-tetradecanoylphorbol-13-acetate (TPA)-induced inflammation and attenuates age-associated oxidative stress in skin, demonstrating both skin regenerative and geroprotective properties of RM191A.

1. Introduction

Our skin acts as the first barrier of defence against various infections, trauma and environmental factors. Risk factors like ultraviolet (UV) radiation, environmental pollutants, xenobiotics, aging, wounds, chronic inflammation and inflammatory skin diseases, such as psoriasis and atopic dermatitis, are major impediments against the proper maintenance of the skin barrier [1–4]. Oxidative stress, which compromises proper skin integrity, is one of the most common features among these various risk factors [5–7]. An over-abundance of oxidants or catalysts producing free radicals, such as reactive oxygen species (ROS) and reactive nitrogen species (RNS), and in parallel the failure of the endogenous anti-oxidant defence system in skin cells, primarily contribute to the formation of oxidative stress in skin [8–10]. Furthermore, oxidative stress and inflammation are closely interconnected pathophysiological processes that are known participants in the pathogenesis of numerous skin diseases [11–14]. Inhibition of oxidative stress and inflammation is therefore important for maintenance of normal skin

* Corresponding author.
E-mail address: abhirupdas@unsw.edu.au (A. Das).

https://doi.org/10.1016/j.redox.2020.101790
Received 29 April 2020; Received in revised form 12 October 2020; Accepted 2 November 2020
Available online 6 November 2020

function.

Superoxide dismutase (SOD) enzymes catalyze the disproportionation of the cytotoxic superoxide ($O_2^{\cdot-}$) free radical to hydrogen peroxide and oxygen and play a significant role in the attenuation of oxidative stress in our body [15]. SODs have been reported to be protective against many skin disorders [16]. They sequester free radicals which are formed following UV exposure and have the potential to damage our DNA. Such DNA damage has been shown to be a major contributing factor to skin carcinogenesis. Due to its powerful antioxidant potential, endogenous SOD also exhibits potent anti-inflammatory activities by inhibiting the expression of ROS-sensitive transcription factors [17]. SOD plays a major role in wound healing [18,19]. For these reasons, exogenous SOD was contemplated as a therapeutic agent for the treatment of various skin disorders. However, the lack of clinical development of exogenous SOD is due to its large size (molecular weight ≈ 30 kDa), low cell permeability, short circulating half-life, antigenicity, and high manufacturing costs [20]. To overcome these issues, much focus has been placed on the synthesis of low-molecular-weight, stable compounds that mimic SOD's antioxidant activity.

There are three kinds of SOD enzymes. SOD2 is localized in mitochondria and contains manganese. Both cytosolic SOD1 and extracellular SOD3 enzymes contain a redox active copper atom (Cu^{2+}), which is fundamental to the dismutation of the superoxide free radical, and a zinc atom [21–23]. Interestingly, it has been established that if the zinc atom of either SOD is replaced with a copper atom, this di-copper form has the same free radical/superoxide scavenging activity as the endogenous Cu/Zn enzymes [24]. A significant number of the SOD mimetics reported in the literature focus on replicating the activity of SOD2. These include a variety of manganese porphyrin complexes, manganese (II) penta-azamacrocyclic complexes, and manganese (III) salen complexes [25]. Topical application of these SOD mimetics demonstrated potential benefits for the treatment of skin disorders [26–28]. Only a small number of SOD mimetics utilising the unique copper-based bivalent configuration of SOD1 have been reported, however, their biological activities were never demonstrated [24,29,30].

Here we report for the first time, a highly stable, unique copper (Cu^{2+}-Cu^{3+})-centred polyglycine coordination complex – RM191A, which has been demonstrated through extensive analytical, *in vitro* and *in vivo* evaluation to possess robust antioxidant, anti-inflammatory and immunomodulatory activities. Our work indicates biological activity of topically applied RM191A across a broad spectrum of skin disorders. Specifically, we report protection of the epidermis, dermis and associated DNA following exposure to UV radiation in human skin explants; acceleration of wound healing; and significant anti-inflammatory and antioxidant activities in the skin of young and old mice. We posit that these activities are a result of the complex's SOD-like activity, immunomodulation and beneficial alteration of a number of important signalling pathways, including attenuation of key inflammatory cytokines.

2. Material and methods

RM191A Synthesis. RM191A was synthesized according to a proprietary protocol patented by RR MedSciences. RM191A gel formulation consists of 21 mg of RM191A in 1 mL of hydrogel base (Vehicle).

Elemental analysis. Elemental microanalysis was performed using 2400 CHNS elemental analyzer (PerkinElmer).

FTIR. FTIR spectroscopy was performed using Nicolet iS5 FTIR Spectrometer (Thermofisher).

Cryo-TEM. After diluting 2 mg of the sample into 1 mL of pure water (500 dilution), the sample (6 μL) was pipetted onto 300 mesh copper grids with a lacey formvar film (GSCu300FL-50, ProSciTech, Australia). The sample droplet was allowed to equilibrate for 30 s at room temperature and 90% relative humidity, before being blotted from one side for 1.8 s. The blotted grid was subsequently plunged into liquid ethane held at −174 °C, excess ethane was blotted away with a piece of pre-cooled filter paper, and the vitrified grid stored in liquid nitrogen. The samples were then analysed by cryo-TEM.

DOSY. The DOSY experiments were carried out on a Bruker AVANCE 400 MHz NMR in D_2O at 25 °C with a BBFO probe using 3-9-19 water suppression.

X-ray crystallography. Blue solid of RM191A was crystallised from supernatant generated by addition of ethanol to reaction mix. Powder diffraction was performed on a Panalytical Empyrean Bragg-Brentano geometry instrument fitted with a cobalt X-ray source.

Measurement of SOD activity. We employed a modified version of the method described by Beauchamp and Fridovich [31]. The objective was to create a reaction mixture that successfully generates known quantities of the $O_2^{\cdot-}$ free radical but does so at a pH at which RM191A is stable (pH 6.5–7.8). Nitro Blue Tetrazolium (NBT) was selected as an indicator to measure and compare the superoxide scavenging activities of both bovine SOD and RM191A. This assay utilized photochemical events to generate $O_2^{\cdot-}$ in a phosphate buffered solution of acetone and isopropanol which was then irradiated by high energy UV light at 254 nm (Mercury Vapour Lamp) to create $O_2^{\cdot-}$ in the solution. SOD and SOD-like substances inhibit the formation of the blue formazan by neutralising the superoxide free radicals as they are forming. Blue formazan has a characteristic UV absorbance at 560 nm. UV absorbances of the reaction solutions were measured at 560 nm following irradiation with UV light to determine the superoxide free radical scavenging activity in situ of both bovine SOD and RM191A. The UV–vis spectrum of both SOD and RM191A did not exhibit any absorbance at 560 nm (Fig. S2B). The reaction solution consists of 0.5 mL of 200 μmol/L NBT in phosphate buffer (pH = 7.8) and 0.5 mL of a 200 μmol/L solution of the test compound in 5.0 mL of 5 mol/L isopropanol. 15 mg acetone (20 μL) was added to begin the reaction. The reaction mixture was placed in UV light at 254 nm (mercury vapour lamp) for 1 min and then transferred to a spectrometer to measure absorbance at 560 nm. The assay was repeated by adding, 1.0, 1.25, 1.5, 1.75, 2.0 mL of a 200 μmol/L solution of the test compound bringing total volume to 5.0 mL with 5 mol/L isopropanol.

Cells. N27 cells were cultured in RPMI 1640 medium supplemented with 10% (v/v) fetal calf serum (FCS), 2 mM L-glutamine and penicillin/streptomycin solution at 37 °C with 5% CO_2. RAW 264.7 cells were cultured in DMEM medium supplemented with 10% FCS and 1% Pen/Strep at 37 °C with 5% CO_2. Human umbilical vein endothelial cells (HUVEC) and hCMEC/D3 were cultured in RPMI + 10% FCS at 37 °C with 3% O_2 and 5% CO_2. Adult normal human dermal fibroblasts (NHDF) were cultured in FGM-2 fibroblast growth medium-2 (Lonza) at 37 °C with 3% O_2 and 5% CO_2. RAW 264.7 cells (10^6) were stimulated with LPS (10 ng/mL) and treated with RM191A (2.1 μg/mL) or Vehicle for 6 or 24 h.

Cell viability. Cell viability was assessed using propidium iodide exclusion assay as described before [32]. Briefly, cells (0.1×10^5 cells) were seeded in a 48-well plate and incubated with different concentrations of RM191A or Vehicle for 24 h. After 24 h, cells were trypsinized, stained with PI (10 μg/mL) and the number of PI negative (PI -ve) cells were determined by flow cytometry (BD FACSCanto II). In hydrogen peroxide-mediated oxidative stress assay, N27 cells were first exposed to 200 μM hydrogen peroxide for 30 min and then treated with 21 μg/mL RM191A (or Vehicle) for 4 h, after which cell viability was measured using flow cytometry. Alternatively, cell viability was determined using MTT assay kit (Sigma Aldrich) according to manufacturer's protocol.

Measurement of intracellular ROS. ROS generation in LPS-stimulated RAW 264.7 cells was determined as previously reported [33]. After 6 h of LPS stimulation, the fluorescent dye CM-H_2DCFDA (final concentration 10 μl of 20 μM) was added to cells and incubated for 30 min in a CO_2 incubator to measure the intracellular ROS produced in these cells. After incubation, the cells were washed with cold phosphate buffered saline (PBS) and the amount of ROS was analysed by flow cytometry.

Measurement of NO. Nitrite concentrations in cell culture supernatants and tissues were determined using a Nitrate/Nitrite Colorimetric

Assay Kit (Cayman Chemical) according to the manufacturer's instructions. In short, nitrate reductase was used to enzymatically convert all nitrate to nitrite. Next, Griess reagents R1 and R2 were used to produce deep purple coloured compound and detected using a plate reader, absorbance at 540 nm. The skin and ear tissue lysates were prepared in PBS with 1% Triton-X and protease inhibitors.

Real-time quantitative PCR. RNA extraction from cells and tissues was performed using a RNeasy Plus Mini Kit (Qiagen) according to the manufacturer's instructions. The cDNA was synthesized using iScript cDNA Synthesis Kit (Bio Rad). PCR amplification of cDNA with gene specific primers was performed using FastStart Universal SYBR Green Master (ROX) (Sigma Aldrich). Fold changes in genes were calculated using delta delta C_T method. HPRT was used as a housekeeper gene. The list of primers is shown in Table S6.

Gene expression analysis. Gene expression in NHDF was performed at Bosch Institute, Sydney. NHDF were treated with RM191A (21 μg/mL) or Vehicle for 24 h. Mature RNA was isolated using an RNA extraction kit (Qiagen) according to the manufacturer's instructions. RNA quality was determined using a spectrophotometer and was reverse transcribed using a cDNA conversion kit (Qiagen). The cDNA was used on the real-time RT^2 Profiler PCR Arrays (QIAGEN, Cat. no. PAHS-065Y, PAHS-022Z, PAHS-162Z) in combination with RT^2 SYBR® Green qPCR Mastermix (Cat. no. 330529). Fold changes in genes were calculated using delta delta C_T method in data analysis web portal (http://www.qiagen.com/geneglobe). The gene expression for each group was analysed in two different experiments. The heat map was generated using Morpheus software (Broad Institute). The C_T cut-off was set to 36.

Blood-brain-barrier transmission assay. hCMEC/D3 cell line derived from human brain endothelial cells were seeded onto membrane of 24 mm Transwells with 4 μm pores (Corning) coated with 3% collagen at 4.5×10^5 cells/well and grown to confluence in RPMI + 10% FCS medium. RM191A was added to the top of the transwell at 8.4, 16.8, 33.6 and 168 μg/mL. After 2 and 6 h, media from top and bottom chambers of the transwells were collected and stored at −20 °C until further analysis. The media was then analysed by HPLC (Phenomenex Luna HILIC Analytical Column 3 μm, 2 × 100 mm, mobile phase: 85/15 ACN/NH_4 formate buffer (0.1 M. pH 4.3)).

UV exposure and RM191A treatment in skin explants. All experiments were performed according to procedures approved by University of Sydney Human Ethics Committee. Human skin explants were obtained with consent from patients undergoing elective surgery. The protocol for obtaining skin explants and for their use to examine photoprotective effects of test agents was described in Song et al., with some minor changes [34]. In brief, skin removed at elective surgery was cleaned, subcutaneous fat removed and cut into pieces to produce multiple pieces approx. 4–6 mm x 4–6 mm, with each explant placed in one well of a 96 well plate in RPMI 1640 media containing 10% FCS. Skin explants in triplicate were used for each treatment point. The DNA damage was analysed after 3 h incubation period.

Skin was subjected to solar simulated UV-radiation, as previously described [34,35]. The spectral output of this solar simulator compared with sunlight is shown in Fig. S3A. Treatments, as indicated below, were applied to the epidermal surface of the explant. Sham wells were treated in a similar manner to UV-exposed wells, including media changes and treatments, but were covered with foil and not exposed to UV. RM191A or Vehicle was used with two protocols. In Protocol 1, 1.5 μL of RM191A/Vehicle was applied to the surface of the explant 10–15 min prior to UV exposure, then again immediately after UV and then at 0.5, 1.5, and 2.5 h. In Protocol 2, 1.5 μL of RM191A/Vehicle was applied to the surface of the explant immediately after UV exposure, then at 1, 2, 2.5 h. The positive control treatment was 1,25 dihydroxyvitamin D3, (1, 25D) [34], which was dissolved in spectroscopic grade ethanol (1,25D Vehicle) at a final concentration of 1 nM and 0.1% v/v ethanol in RPMI media with 10% v/v FCS. Both 1,25D and 1,25D Vehicle were also applied immediately after UV. Sham wells consisted of 1,25D Vehicle, 1, 25D, Vehicle 1 (Protocol 1 only) and RM191A 1 (Protocol 1 only). There were insufficient explants to do sham wells of RM191A and Vehicle with Protocol 2 at both time points. UV-exposed wells consisted of 1,25D Vehicle, 1,25D, Vehicle 1, Vehicle 2, RM191A 1 and RM191A 2.

Animal experiments. All experiments were performed according to procedures approved by University of New South Wales (UNSW) Animal Care and Ethics Committee. Male C57BL/6 mice (Australian Bio-Resources, Mossvale, NSW and Animal Resource Centre, Canning Vale, WA, Australia) were housed in the UNSW Biological Resource Centre (BRC) at 21 °C ± 2, with a 12 h/12 h dark/light cycle and were fed standard chow diet.

RM191A treatment. One day prior to the application of RM191A, male mice were anaesthetised and hair on the dorsal surface was removed with a clipper. The shaved area was then cleaned with betadine solution, wiped with an alcohol swap and dried for a few seconds. The following day, the animals were briefly anaesthetised and RM191A at different concentrations (diluted in gel to make up to 50 μL) was applied topically. This step was repeated for 3 and 29 consecutive days for short-term and long-term treatment protocols, respectively. On the 4th and 30th day, the animals were euthanized, tissues were harvested, and flash frozen in liquid nitrogen. The overall health of the animals was monitored daily and weights were recorded daily until euthanized. For the short-term treatment protocol, the treatment groups consisted of Vehicle and RM191A (0.19, 0.38, 0.76, 1.33 and 1.9 mL/kg). For long-term treatment protocol, the groups consisted of no gel, Vehicle and RM191A (0.19 mL/kg). Aged (102-week-old) female mice were shaved dorsally and 50 μL of RM191A (0.38 mL/kg) or Vehicle was applied topically for 7 consecutive days. The animals were euthanized on the 8th day.

Teratogenicity study. Two females and a male (12 weeks of age) were housed in a cage for mating overnight and maintained on a 12-h light/dark cycle. The females were examined for the presence of vaginal plugs the following morning. If a plug was observed then the onset of gestation (gestation day GD 0) was considered to be 1:00 a.m. of the previous night, the midpoint of the dark cycle. On GD 4, the dam was weighed, dorsal surface was shaved and transferred to a separate cage for single housing for the rest of the period. RM191A (5 μL of 21 mg/mL RM191A in 45 μL of gel) was administrated daily dorsally until GD18. On GD19, all dams were euthanized by CO_2 and the uterus with pups were removed. The maternal weight gain was determined by subtracting the body weight on GD0 from GD18. The litters were assessed by counting and measuring the weight. The morphology of litters was determined by μ-CT analysis (U-CT MILabs) after fixation in 10% formalin.

Rotarod test. Motor coordination was assessed using the rotarod test as previously described [36]. In short, mice were acclimatized to a rotarod for 3 days in three trials lasting 2 min each at a constant speed of 5 rpm. On the 4th day, the animals were subjected to three trials on the accelerating roller (4–40 rpm in 4 min) and the time that the mice remained was recorded.

Rearing test. Mouse rearing test was performed as described previously [37]. Briefly, the mouse was placed in a clean transparent cylinder (diameter: 12 cm, height: 15 cm) for 3 min and its forelimb activity while rearing against the wall of the arena was recorded.

EchoMRI. Body composition (fat mass, lean mass, and total body water) was measured by EchoMRI (EchoMRI-900).

RM191A time point study. One day prior to the application of RM191A on mice, the animals were anaesthetised and hair on the dorsal surface was removed with a clipper. The shaved area was then cleaned with betadine solution, wiped with alcohol swap and dried for a few seconds. Next day, the animals were briefly anaesthetised and 50 μL of RM191A in gel formulation (1.9 mL/kg RM191A) was applied topically. The animals were euthanized at 0, 15 min, 30 min, 1 h and 2 h post-treatment and tissues were harvested.

ICP-MS. About 100 mg of tissue sample (50 μL in the case of plasma and urine) was transferred to a 10 mL polypropylene tube (Sarstedt), then 200 μl of concentrated nitric acid (HNO_3) was added and incubated

for 12 h at room temp with occasional shaking. After 12 h, the tube was heated at 80 °C moderately up to clearing (5 h) and cooled down to room temperature. 20 μl of hydrogen peroxide was added, and the tube was again heated up to 80 °C for 2 h. Next, the volume was made up to 10 mL with milliQ water. A blank standard was prepared in the same way. The samples were then analysed for copper using ICP-MS NEXion (PerkinElmer).

Ear edema model. TPA (12-O-tetradecanoylphorbol-13-acetate)-induced mouse ear edema was generated according to a published protocol [38]. Briefly, 6 μg of TPA dissolved in 20 μL acetone was applied to the left ear of a mouse. 20 μL of acetone was applied to the right ear as vehicle control. Both ears were pre-treated with 50 μL of Vehicle or RM191A (2.1 mg/mL), 15 min prior to TPA or acetone application, and 10 min after TPA or acetone application. After 6 h, ear tissue was excised using a 5 mm biopsy punch and ear weight was measured. The ear samples were then fixed in 10% formalin or kept frozen at -80 °C.

Wound regeneration model. Wound healing protocol in mice was performed as described previously, with minor modifications [39]. One day prior to wounding, the animals were anaesthetised and hair on the dorsal surface was removed with a clipper. The shaved area was then cleaned with betadine solution, wiped with an alcohol swab and dried for a few seconds. Next day, the animals were briefly anaesthetised, and a wound was created on the dorsal skin using a 10 mm biopsy punch. The picture of wound was captured, and the wound was covered with a semi-occlusive dressing (3 M Tegaderm). Two days after the wounding procedure, 50 μL of Vehicle or RM191A (2.1 mg/mL) was applied to the wound area and the application was repeated every 2 days. Each animal was singly housed during the entire procedure. The pictures of wounds were captured every 2 days and wound area was analysed using ImageJ software.

Hematoxylin and eosin (H&E) staining. After fixation in paraffin, samples were stained with 0.1% Hematoxylin for 10 min, rinsed with dH_2O, stained with Scott's blue solution for 1 min and then washed with dH_2O. The sections were then dipped in Eosin for 3 min, dehydrated through alcohol and cleared in xylene. The slides were mounted with DPX and imaged using a Zeiss Axio Scan Z1 (Zeiss) slide scanner.

Toluidine blue staining. After fixation and subsequent paraffin embedding, samples were dewaxed and washed in dH_2O. Sections were then stained with toluidine blue solution (0.1% in PBS, pH 2.0–2.5) for 3 min. The sections were then dehydrated and cleared in xylene. The slides were then mounted with DPX and imaged using an electronic microscope.

Masson trichrome staining. Following fixation, sections were stained with Bouin's solution for 1 h at 56 °C, rinsed in dH_2O and subsequently stained through repeated dips of Celestine blue, Harris hematoxylin, Scott's blue, Acid alcohol, Scott's blue and Briebrich Scarlet. Next, the slides were rinsed in dH_2O and left in 1% Phosphomolybdic acid until collagen decolourisation became apparent and stained further in Light green/Aniline blue, 1% acetic acid with quick dH_2O washes between each stain. The slides were then mounted with DPX and imaged using an electronic microscope.

Immunohistochemistry. Three or 24 h after irradiation, the huma skin explants were fixed, embedded in paraffin and sectioned before being deparaffinized and rehydrated for staining. Antigen retrieval was achieved with 10 mM citrate buffer. These sections were then stained as described for cyclobutane pyrimidine dimers (CPD), oxidative DNA damage in the form of 8-oxo-guanine (8-oxoG) and nitrosative DNA damage in the form of 8-nitroguanine (8NGO) [34]. Isotype controls were performed (without primary antibody). Immunohistochemistry was carried out and analysed using the Metamorph image analysis program as previously described [34], except that the results were expressed as mean pixel intensity – mean grey value in arbitrary units [35]. In addition to analysing nuclear staining in the epidermis, for 8-oxoG and 8NGO, a separate analysis was performed on the upper layer of the dermis, where there were reasonable numbers of cells visible.

Multiplex assay. Custom murine Luminex immunoassays for GRO-α, IL-1β, IL-6 and MCP-1 in cell culture supernatants and mouse serum were performed by Crux Biolabs (Bayswater, Australia).

Statistics. Data are presented as mean ± SEM. Statistical significance was performed using Student's t-test or ANOVA with Tukey's *post hoc* test. Statistical tests were performed using GraphPad Prism software. P values of less than 0.05 were considered statistically significant.

3. Results

3.1. Synthesis and characterization of RM191A

Synthesis of RM191A yielded a dark blue-green aqueous solution, and when dried the compound contains 11.8% copper (Fig. 1A, Table 1). RM191A is a highly polar compound that is completely insoluble in non-polar solvents. Although the UV–visible absorption spectra of RM191A was similar to that of Cu-EDTA complex (Fig. S1A), RM191A exhibited an intense fluorescence emission peak at 440 nm (Fig. 1B). FTIR spectra of RM191A showed absorbances characteristic of amino and carboxylic acid functionalities (Fig. S1B). This information combined with the elemental analysis indicate that RM191A is a copper-amino acid chelate complex.

To delineate the structure further, analysis via cryo-TEM was performed in which RM191A showed unexpected black dots about 20–50 nm in diameter in comparison with a blank sample, strongly suggesting the presence of large copper-containing complexes in this sample (Fig. 1C). This conclusion was also supported by NMN diffusion ordered spectroscopy (DOSY), in which the compound exhibited a large apparent increase in the chelate hydrodynamic radii suggesting that the proton signals seen in the ^{1}H NMR of the copper chelate complex belong to a species that is oligomeric (Table 2, Fig. S1C). The hydrodynamic radius of Cu species in RM191A appeared to be at least 4.67 Å or a diameter of nearly 1 nm compared to 3.0 Å radius (0.6 nm diameter) for a standard Zn-EDTA complex. X-ray diffraction of crystalline RM191A showed a hydrated copper-polyglycine coordination complex where glycine-like ligands are shared between two copper atoms, resulting in a square planar and pyramidal geometry (Fig. 1D, Fig. S1D). Diffusion pulsed voltammetry confirmed the presence of both Cu^{2+} and Cu^{3+} ions in RM191A (Fig. 1E, Fig. S1E). Together, this data confirmed that RM191A was a Cu^{2+} and Cu^{3+} containing polyglycine coordination complex.

3.2. RM191A has potent antioxidant and anti-inflammatory properties

The interesting similarity of RM191A to the dimeric structure of SOD1 and presence of unique Cu^{2+}/Cu^{3+} dipole led us to postulate that RM191A would be a highly efficient free radical scavenger, which could act in a similar manner to SOD. To prove our hypothesis, we measured and compared the superoxide scavenging activities of both bovine SOD and RM191A using a well-established assay [31]. The results showed that at 20 μM concentration, RM191A was 10 times more effective at neutralising superoxide free radicals than SOD (Fig. 2A). At 40 μM, the activity of RM191A exceeded that of SOD by 30 times. With increasing concentration, RM191A maintained the same neutralising activity, however, that of SOD decreased (Fig. S2A). This is not surprising as it has been reported that the ratio of antioxidant/pro-oxidant effects of SOD decreases as its concentration increases [40].

Next, we decided to test the bioactivity of RM191A in cells. For all subsequent experiments, RM191A was dissolved in a hydrogel (Vehicle). Upon treatment of N27 cells, an immortalized rat dopaminergic neuronal cell line [41], with different concentrations of RM191A and measuring the percentage of live cells by flow cytometry or MTT assay, the LD_{50} of RM191A was observed to be 210 μg/mL (Fig. 2B, Fig. S2C). Similarly, LD_{50} of RM191A for human umbilical vein endothelial cells (HUVEC) was found to be 210 μg/mL (Fig. S2D). In order to determine if RM191A could protect cells from ROS-mediated oxidative stress, N27

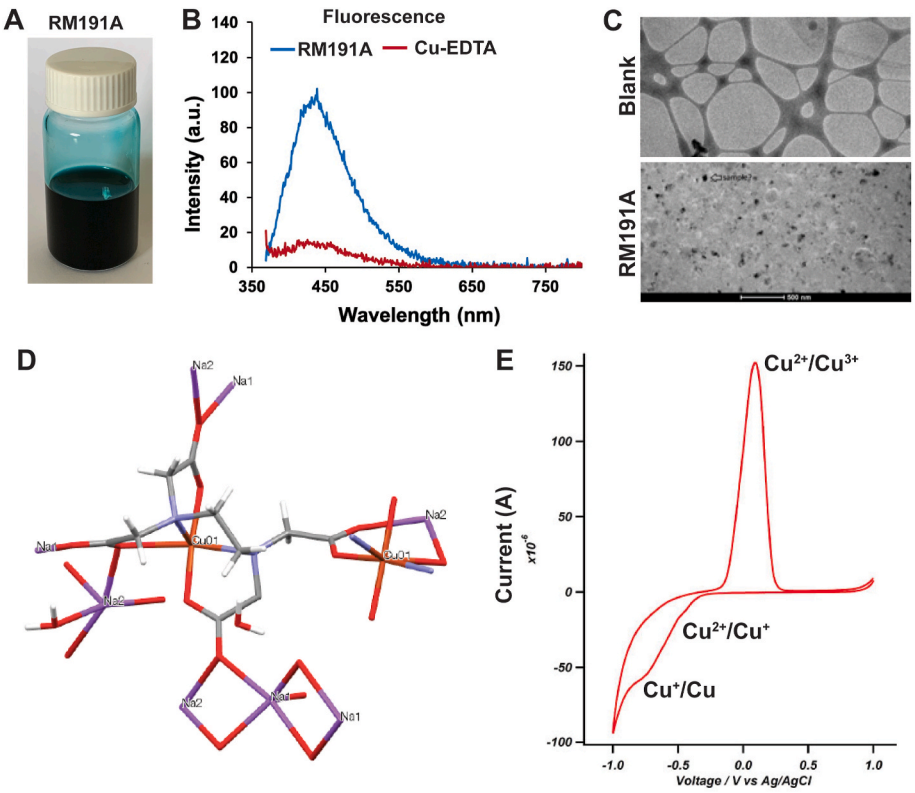

Fig. 1. Synthesis and characterization of RM191A. (A) Picture of RM191A solution. (B) Fluorescence emission spectrum of RM191A and Cu-EDTA with peak at 440 nm. (C) Cryo-TEM images of blank (top) and RM191A (bottom). (D) Structure of RM191A crystal from X-ray single-crystal analysis (Red = oxygen, blue = nitrogen, light red = copper, dark grey = carbon, light grey = hydrogen). (E) Cyclic Voltammogram of RM191A solution showing two reduction peaks and one oxidation peak. (For interpretation of the references to colour in this figure legend, the reader is referred to the Web version of this article.)

Table 1
Elemental analysis of RM191A.

Element	Cu	C	H	N	Na	O
%	11.8	27.46	4.45	7.06	12.0	37.23

Table 2
DOSY analysis of RM191A and Zinc-EDTA complex.

Compound	log(D) (m2S-1)	Hydrodynamic radius (m)	Hydrodynamic volume (m3)	Relative volumes
Zinc-EDTA	−9.09	3.02×10^{-10}	1.15×10^{-28}	1
RM191A	−9.28	4.67×10^{-10}	4.27×10^{-28}	3.7

cells were first exposed to 200 μM hydrogen peroxide for 30 min and then treated with 21 μg/mL RM191A (or Vehicle) for 4 h. RM191A treatment increased the viability of cells by 24% when measured by flow cytometry, compared to the control (Fig. 2C).

ROS is known to mediate inflammatory responses induced by a variety of stimuli including lipopolysaccharide (LPS) [42,43]. Treatment of macrophage-like RAW 264.7 cells with exogenous SOD decreases LPS-induced ROS and RNS generation as well as down-regulates several inflammatory genes, including IL-1β, IL-6 and TNF-α [43,44]. To investigate if RM191A has similar effects, at first, we determined its toxicity in RAW 264.7 cells using flow cytometry and MTT assay. The LD_{50} of RM191A was 85 μg/mL in both assays (Fig. S2E, S2F, S2F). Next, RAW 264.7 cells were stimulated with LPS (10 ng/mL) and then treated with RM191A (2.1 μg/mL) or Vehicle only. After 6 h the amount of ROS was measured by flow cytometry. LPS stimulation resulted in a 42% increase in ROS level and treatment with RM191A decreased it to 36% (Fig. S2G). The production of RNS was determined by measuring the nitrous oxide (NO) level in the culture medium using Griess reagent. As shown in Fig. 2D, LPS induced a 15-fold increase in NO production after 24 h in the Vehicle-treated group when compared to unstimulated RAW cells (Fig. 2D). However, RM191A treatment of LPS-stimulated group reduced the NO level by 75% compared to LPS/Vehicle-treated group. The mRNA levels of pro-inflammatory cytokines IL-1β, IL-6 and TNF-α were analysed by real time-quantitative PCR at 24 h. RM191A significantly inhibited the expression of these cytokines, with that of TNF-α being reduced by 80% in LPS-stimulated groups (Fig. 2E). The inhibition of IL-1β was also observed in the protein level, where multiplex assay using the culture medium demonstrated an 89% reduction in IL-1β secretion from RM191A treated cells upon LPS stimulation when compared to the control (Fig. 2F). Although the mRNA level of NLRP3 inflammasome was upregulated in LPS-stimulated, RM191A-treated cells compared to the control (Fig. S2H), it has been previously reported that RAW cells are defective in activation of NLRP3 due to the lack of ASC protein adaptor [45].

Given these data, we were curious to understand RM191A's ability to affect oxidative stress and inflammatory pathways. To investigate this, adult normal human dermal fibroblasts (NHDF) were treated with RM191A and changes in gene expression in an unstimulated state compared to control were determined using PCR arrays. Toxicity analysis demonstrated that RM191A was well-tolerated by NHDF, with no evident cell death up to a dose of 210 μg/mL (Fig. S2I). Although RM191A treatment did not change the expression of SODs in NHDF, the expression of several genes that confer cellular protection against oxidative stress were significantly upregulated (Fig. S2J, Table S1). Notably, heme oxygenase (HMOX1), heat shock protein (HSPA1A) and thioredoxin reductase (TXNRD1) expression increased by 70, 7 and 5-fold respectively in RM191A-treated NHDF compared to the control. Amongst the inflammatory genes, CCL7, CXCR6, CCRL1 and CMKLR1 were downregulated, while the expression of CCL26 and IL8 were upregulated in RM191A-treated NHDF (Fig. S2K, Table S2). These small changes in chemokines may be due to the fact that in basal condition, the inflammatory genes are not upregulated in NHDF and therefore the protective effects of RM191A were not obvious. Repeating the experiment where the NHDF are subjected to oxidative stress by external stimuli would be ideal to demonstrate the anti-inflammatory effects of

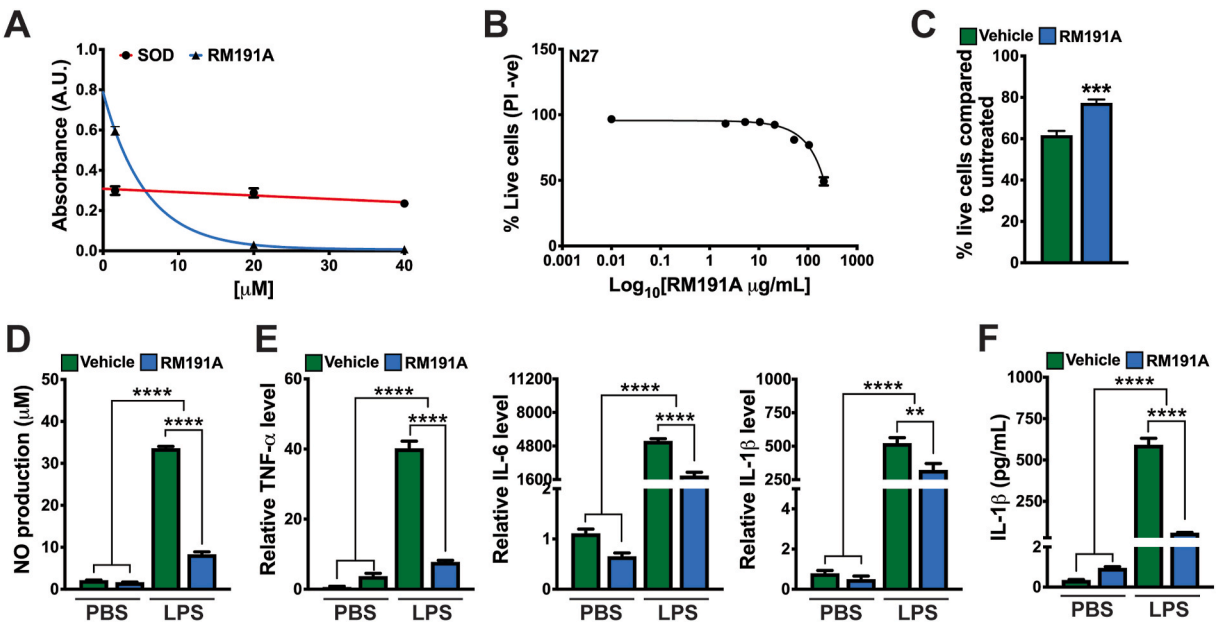

Fig. 2. RM191A has potent antioxidant and anti-inflammatory properties.
(A) Comparison of superoxide scavenging activities of both bovine SOD and RM191A between 1.6 and 40 μM concentration at 560 nm (n = 3). (B) Dose-response curve of RM191A for N27 cells, as measured by PI exclusion (PI -ve) in flow cytometry (n = 6). The median lethal dose (LD_{50}) is 210 μg/mL. (C) Percentage of live N27 cells, as measured by PI exclusion (PI -ve) in flow cytometry, exposed to 200 μM hydrogen peroxide for 30 min and then treated with 21 μg/mL RM191A or Vehicle for 4 h (n = 6). (D) Amount of nitrous oxide (NO) generated by RAW 264.7 cells upon LPS (10 ng/mL) stimulation, followed by treatment with RM191A (2.1 μg/mL) or Vehicle for 24 h (n = 6). NO level was determined by measuring the nitrite in culture medium using Griess reagent. (E) Relative IL-1β, IL-6, TNF-α mRNA levels in RAW 264.7 cells upon LPS (10 ng/mL) stimulation, followed by treatment with RM191A (2.1 μg/mL) or Vehicle for 24 h (n = 3). HPRT gene was used as a reference. (F) Amount of IL-1β secreted in the culture medium, upon LPS stimulation of RAW 264.7 cells, followed by treatment with RM191A (2.1 μg/mL) or Vehicle for 24 h (n = 4).
Data expressed as mean ± SEM. **p < 0.005, ***p < 0.0005 and ****p < 0.00005 by *t*-test.

RM191A. Since inflammation also contributes to pain [46], we then measured the effects of RM191A on pain-associated genes. Several key biomarkers of pain, for example, IL-18, BDNF and serotonin receptor (HTR2A) were downregulated in NHDF upon RM191A treatment (Fig. S2L, Table S3).

In conclusion, RM191A possesses significant antioxidant and anti-inflammatory properties via regulation of ROS, RNS and several key signalling pathways.

3.3. *RM191A protects skin against UV-induced oxidative stress and DNA damage*

Exposure of skin to UV radiation induces direct DNA damage such as generation of cyclobutane pyrimidine dimers (CPD), as well as oxidative stress via a dramatic increase in ROS and RNS (Fig. S3B) [47]. Such an increase results in characteristic DNA damage, for example, oxidative DNA damage in the form of 8-oxo-guanine (8-oxoG) and nitrosative DNA damage in the form of 8-nitroguanine (8NGO) [48]. If these DNA lesions are inadequately repaired, mutations can occur and may lead to the development of skin tumours [48]. We wanted to determine whether RM191A, when applied topically to *ex vivo* human skin, reduced UV-induced DNA damage.

Human skin was either pre-treated with RM191A (RM191A 1), followed by exposure to UV radiation, or treated with RM191A (RM191A 2), immediately after UV exposure. In both cases, RM191A treatment post-UV exposure was repeated every 30 min for 3 h incubation period. The same treatment protocols were also followed for Vehicle. An active form of vitamin D – 1,25-dihydroxyvitamin D3 (1,25D), was used as a positive control in these experiments as it has previously been shown that topical application of 1,25D reduces UV-induced DNA damage in human skin cells, human skin explants and human subjects, and reduces UV-induced skin tumours in mice [49,50]. Ethanol (1,25D Vehicle) was used as a control for 1,25D treatment. Staining for CPD, was virtually absent in the isotype control, and the intensity of nuclear staining was low in the sham exposed explants, indicating very few CPDs (Fig. S3C). This was expected, since exposure to UV was the major source of the energy required to produce CPD. Exposure to UV significantly increased CPD in UV-1,25D Vehicle or UV-Vehicle groups compared with their respective sham controls (compare Fig. 3A and Fig. S3C). Treatment of UV-exposed explants with 1,25D or RM191A (RM191A 2) decreased CPD by 30% compared to their respective UV-exposed controls (Fig. 3A). When pre-treated with RM191A (RM191A 1), CPD decreased by 37% compared to its control (Fig. 3A).

The intensity of nuclear 8-oxoG staining, which is widely recognized as a biomarker of oxidative stress [51], was moderate in the sham exposed explants treated with 1,25D Vehicle or 1,25D (Fig. S3D) due to the fact that culture of the explants engendered some oxidative stress. Markedly increased cytoplasmic staining was seen in explants which were sham exposed and treated with either Vehicle or RM191A (Fig. S3D). Because of this high level of cytoplasmic staining, which was also observed in UV exposed explants, for the analysis, two separate masks (cytoplasmic and nuclear) were created using the Metamorph image analysis program and only the nuclear staining was imaged, so as not to include this strong background, non-specific cytoplasmic stain. Exposure to UV significantly increased nuclear 8-oxoG in both the UV-1, 25D Vehicle and UV-Vehicle groups compared with their respective sham controls (compare Fig. S3D and Fig. 3B). Treatment of UV-exposed explants with 1,25D decreased nuclear 8-oxoG by 27% compared to their UV-exposed controls. Treatment with RM191A (RM191A 2) was found to decrease 8-oxoG levels by 33%, and the RM191A pre-treated group (RM191A 1) was found to have 55% less 8-oxoG, when compared to UV-exposed controls (Fig. 3B). Interestingly, oxidative DNA damage in the nuclei of epidermal cells was lower in RM191A-treated sham explants compared to Vehicle-treated sham

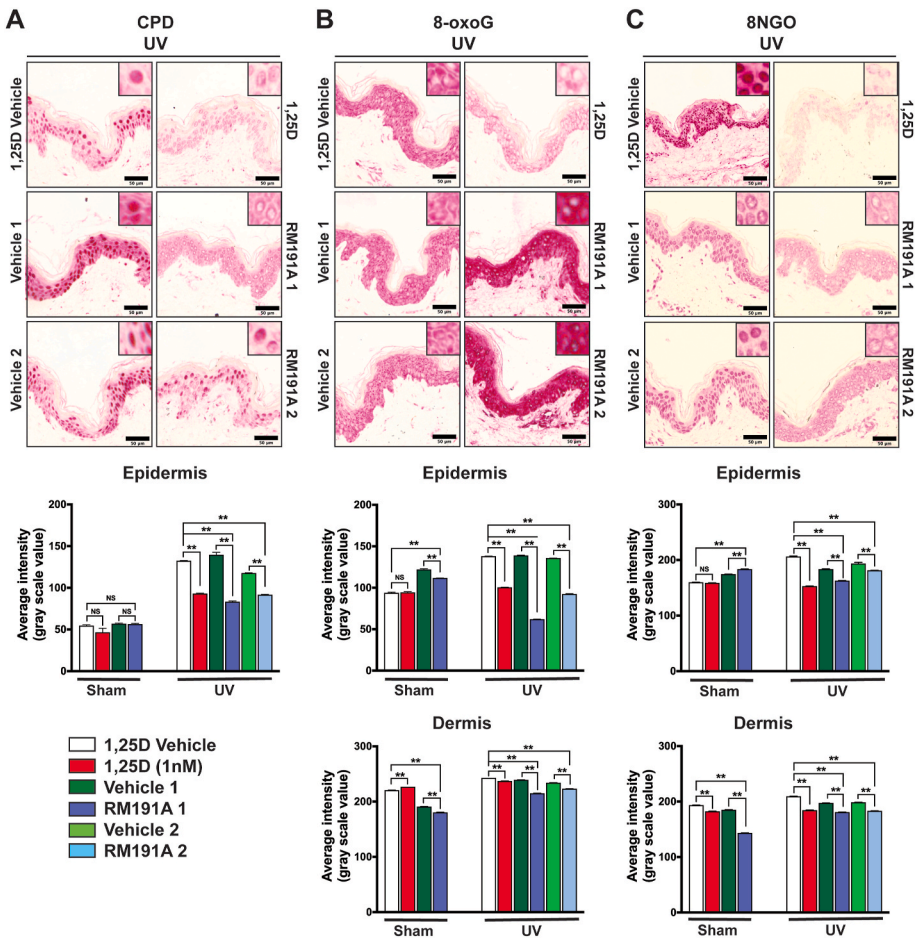

Fig. 3. RM191A protects against UV-induced oxidative stress and DNA damage.
(A) Representative images of immunohistochemical staining of cyclobutane pyrimidine dimers (CPDs) in human skin explants from UV-exposed explants treated with 1,25-dihydroxyvitamin D3 (1,25D), 1,25D Vehicle, RM191A (Protocols 1 and 2) or Vehicle (Protocols 1 and 2) for 3 h. Analysis of CPDs in epidermis of skin explants are shown at the bottom. (B) Representative images of immunohistochemical staining of 8-oxo-guanine (8-oxoG) in human skin explants from UV-exposed explants. Analysis of 8-oxoG in epidermis and dermis of skin explants are shown below. (C) Representative images of immunohistochemical staining of 8-nitroguanine (8NGO) in human skin explants from UV-exposed explants. Analysis of 8NGO in epidermis and dermis of skin explants are shown below. The magnified (120X) images of each staining are shown in the insets. The red stain in the 8-oxoG is in the cytoplasm and the nuclei in the RM191A-treated groups are considerably less stained.
Data expressed as mean ± SEM. **$p < 0.001$ and NS = not significant by One-way ANOVA between data sets (n = 3 explants per data point). (For interpretation of the references to colour in this figure legend, the reader is referred to the Web version of this article.)

wells, indicating that RM191A was able to reduce even base-level oxidative damage. There were far fewer cells in the dermis of the explants, but an analysis was performed on the intensity of staining in the nuclei of cells of the upper dermis. Nuclear staining for 8-oxoG was overall lower in the dermis of sham exposed explants than in UV-exposed explants, but it was not negligible (Fig. 3B). Pre-treatment of sham explants with RM191A significantly reduced 8-oxoG staining. Nuclear stain for 8-oxoG was significantly increased in the dermis in 1, 25D Vehicle and Vehicle treated UV-exposed explants, compared with sham exposed controls, though the fold increase with UV was not as great as seen in the epidermis, probably reflecting reduced penetration of UV into the dermis. Nevertheless, as shown in Fig. 3B, each of the active treatments significantly reduced 8-oxoG in the dermis.

Similar to 8-oxoG staining, exposure to UV significantly increased nuclear 8NGO staining in UV-1,25D Vehicle and UV-Vehicle groups, in both the epidermis and dermis, compared with their respective sham controls (compare Fig. S3E and Fig. 3C). As shown in Fig. 3C, treatment of UV-exposed explants with 1,25D or with RM191A using either protocol significantly decreased 8NGO compared with their UV-exposed controls. Again, pre-treatment of UV-exposed explants with RM191A was more effective at reducing nitrosative DNA damage than RM191A post-treatment.

In conclusion, RM191A was effective in attenuating UV-induced oxidative stress and DNA damage in skin.

3.4. *RM191A is non-toxic, non-teratogenic and readily bioavailable in mice*

After determining the biological activities of RM191A in cells and skin explants, we sought to determine if these effects can translate *in vivo*. Firstly, we used a mouse model to test if RM191A has any toxicity in animals. The dorsal surfaces of 12-week-old male mice were shaved and 50 μL of RM191A at different doses (0.19–1.9 mL/kg body weight) was applied topically daily for 4 days. We found that there were no significant changes in the body weight or tissue weights of these animals compared to Vehicle control after 4 days of topical treatment (Fig. 4A, Table S4), implying that short-term treatment of RM191A is well tolerated in mice up to a concentration of 1.9 mL/kg body weight.

Next, we studied if RM191A was also well tolerated over long-term treatment. As previously, the dorsal area of 8-week-old mice was shaved, and the animals were either left untreated or treated topically daily with 50 μL of Vehicle or RM191A at 0.19 mL/kg body weight for 29 days. No significant changes in body weight, water intake or food intake were observed between the three groups (Fig. 4B, Fig. S4A). The fat content, lean mass and water content, as measured using EchoMRI, were similar among these three groups (Fig. S4B). After confirming that RM191A treatment did not have any adverse impact on the general health of mice, we explored if its exposure altered the behaviour of mice. In a standard rotarod test, the animals from all three groups performed equally well, indicating no significant impact on the motor coordination of mice (Fig. S4C). Both Vehicle and RM191A-treated groups exhibited higher spontaneous rearing behaviour compared to the untreated group (Fig. S4D). Although this increase was not significant, it implied that the Vehicle might improve exploratory behaviour of mice. In order to confirm that there was no overt toxicity in the tissue of various organs, wet tissue weights were measured, and no differences between treated and control groups were observed (Table S5). Furthermore, histological analyses of these tissues by hematoxylin and eosin (H&E) staining showed normal morphology across all groups (Fig. S4E).

Following up on the results from the toxicity studies and skin explant

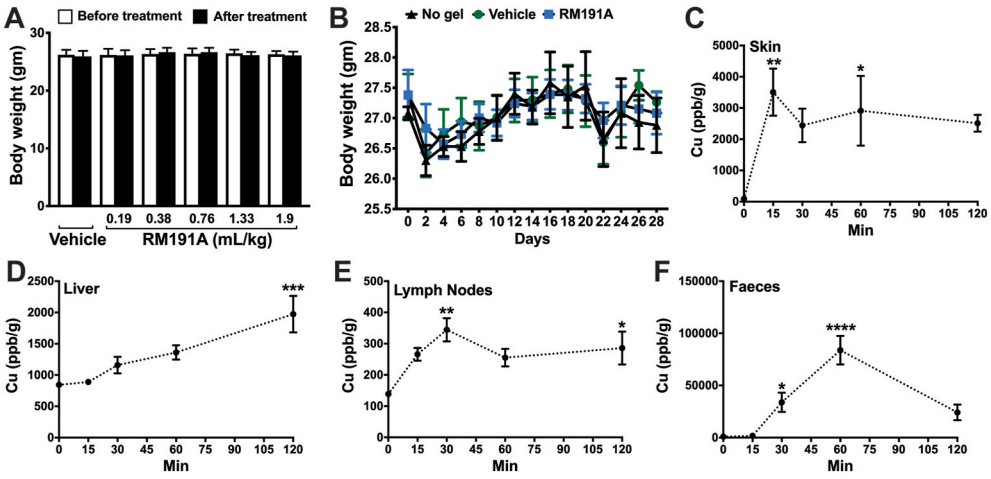

Fig. 4. RM191A is non-toxic and readily bioavailable in mice. (A) Body weights (g) of mice treated daily with different topical doses of RM191A or Vehicle for 4 days (n = 5). (B) Body weights (g) of mice treated daily with topical doses of RM191A (0.19 mL/kg) or Vehicle for 29 days (n = 9). Copper levels in (C) skin, (D) liver, (E) lymph nodes and (F) faeces of mice treated with RM191A (50 μL, 1.9 mL/kg body weight), harvested over different time points and measured using ICP-MS (n = 4 per time point).
Data expressed as mean ± SEM. *p < 0.05, **p < 0.005, ***p < 0.0005 and ****p < 0.00005 by One-way ANOVA.

experiments, we further explored RM191A's ability to penetrate through the skin into the body. The primary goal was to determine whether or not RM191A remained on the skin where it could be washed away, or if it penetrated through the skin into the blood. To gain these insights, we applied 50 μL of RM191A (1.9 mL/kg body weight) topically to the shaved dorsal surfaces of 8-week-old mice and measured total copper content in different animal tissues at different time points using ICP-MS. As expected, the amount of copper in the skin steadily increased within 15 min and stayed steady up to 2 h following RM191A treatment (Fig. 4C). There was also a significant increase in copper levels in internal tissues, including liver, lymph nodes and kidney (Fig. 4D and E, Fig. S4F), which implied that topically applied RM191A was able to penetrate through the skin layers and into the bloodstream (Fig. S4G). The ICP-MS results demonstrated that the copper in RM191A follows the common mammalian metabolic route, with most of the copper being metabolized by the liver, the remainder by the kidneys and was excreted within one hour via the faeces (Fig. 4F) and urine (Fig. S4H). Moreover, the copper was cleared from the body within 24 h as its levels in tissues and blood collected 24 h after RM191A application reduced to the same level as the control group at this time point (Table 3). The changes in brain copper levels indicated that RM191A might be able to cross the blood-brain-barrier (Fig. S4I). This was further investigated using a standard *in vitro* model for human blood-brain-barrier transmission which demonstrated that 50.79% of RM191A at 168 μg/mL concentration crossed the BBB in 2 h, and 95.65% crossed the BBB within 6 h (Fig. S4J).

Since excess copper levels have been associated with birth defects because of oxidative damage caused by accumulation of copper *in utero* [52], we assessed the teratogenic effects of RM191A. Pregnant mice were topically treated or untreated daily with 50 μL of Vehicle or RM191A (2.1 mg/mL) until gestational day 18 and the pups were analysed. In all three groups, no differences in the number of litters, their weight or maternal weight gain were observed (Fig. S4K). Morphological analysis of the pups using μ-CT demonstrated no overt skeletal defects, indicating that RM191A did not have any adverse effects on embryonic development (Fig. S4LL). Overall, RM191A was found to be well-tolerated in mice at varying concentrations and was readily distributed systemically upon topical application.

Table 3
Copper contents (ppb/μL[a] or ppb/g[b]) in plasma and tissues 24 h after RM191A or Vehicle treatment in mice.

	Plasma[a]	Liver[b]	Kidney[b]	Brain[b]
Vehicle (n = 9)	0.173 ± 0.007	744.05 ± 112.01	626.46 ± 23.11	486.18 ± 37.02
RM191A (n = 9)	0.170 ± 0.005	826.02 ± 203.66	591.74 ± 30.46	543.56 ± 102.60

3.5. *RM191A attenuates skin inflammation, improves wound healing and reduces age-associated oxidative stress in mice*

Our previous *in vitro* data demonstrated that RM191A exhibits potent anti-inflammatory activity via suppression of ROS/RNS overproduction and downregulation of various pro-inflammatory signalling pathways. To test this *in vivo*, we employed a TPA (12-O-tetradecanoylphorbol-13-acetate)-induced mouse ear edema model to evaluate the anti-inflammatory activity of RM191A in mice [53]. TPA application increased the ear weight of Vehicle-treated mice by 133% compared to acetone-treated control (Fig. 5A). When the mice were treated with RM191A (50 μL of 2.1 mg/mL), there was only a 35% increase in ear weight after TPA application. H&E staining of TPA-exposed ear cross-sections exhibited a 3-fold increase in ear thickening in Vehicle-treated group, but only 1.4-fold increase in RM191A-treated mice when compared to acetone-treated mice (Fig. 5B). TPA-induced ear edema is also characterized by an influx of immune cells such as leukocytes and mast cells, which markedly enhance the inflammatory response [54]. Upon closer examination of the H&E stains, we observed a 16-fold increase in the number of leukocytes in TPA/Vehicle-treated mouse ears and 6-fold increase in TPA/RM191A-treated group compared to acetone-treated group (Fig. 5B). The number of mast cells was detected by toluidine blue staining of the ear sections. Similar to leukocytes, mast cell numbers increased by 2.7 times in TPA/Vehicle-treated group compared to acetone-treated group, but only 1.3 times in TPA/RM191A-treated group (Fig. 5C). As we have shown previously (Fig. 2D) that activation of immune cells involves the release of NO, we measured the NO levels in ear tissue homogenates from these mice. Consistent with this, TPA/Vehicle and TPA/RM191A-treated groups had 2.8 and 1.8-fold increase in NO level respectively, compared to acetone-treated group (Fig. 5D).

Next, we tested the effect of RM191A in wound regeneration in mice. A circular wound of 10 mm diameter was created on the dorsal surfaces of 12-week-old male mice, after which 50 μL of RM191A (2.1 mg/mL) or Vehicle was topically applied every 2 days to the wound area. Only two days after the start of RM191A treatment, 31% wound regeneration was observed in RM191A-treated group compared to only 12% wound closure in the control group (Fig. 5E). After 12 days, 93% of the skin was regenerated in the RM191A-treated animals, whereas 77% of the wound area was healed in Vehicle-treated mice. H&E staining of the wound areas at 12 days showed regeneration of both epidermis and dermis layers in RM191A-treated group, whereas incomplete restoration of skin layers was observed in the Vehicle-treated group. These results were corroborated by reduction in epidermal gap, increase in epidermal

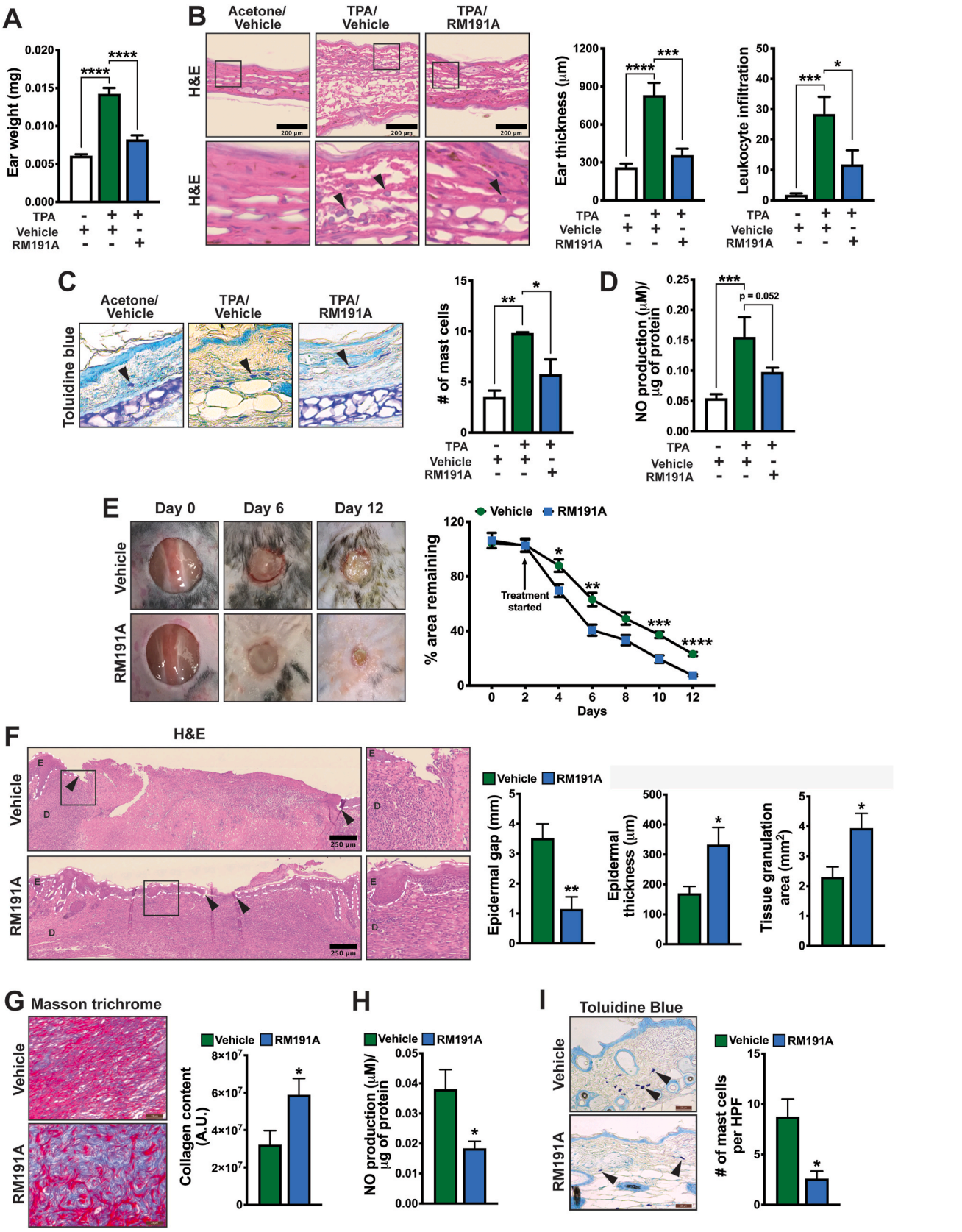

(caption on next page)

Fig. 5. RM191A attenuates skin inflammation, improves wound healing and reduces age-associated oxidative stress in mice.
(A) Ear weights of mice treated with ± TPA (6 μg in 20 μL acetone), and with RM191A (50 μL of 2.1 mg/mL) or Vehicle (n = 6). (B) Representative H&E staining images of ear sections from acetone/Vehicle, TPA/Vehicle and TPA/RM191A treated mice. The magnified views of selected ear areas (black boxes) are shown at the bottom. The arrowheads indicate the infiltrated leukocytes. Quantification of ear thickness and number of infiltrated leukocytes are shown in the right (n = 4). (C) Representative Toluidine blue stains of ear sections from acetone/Vehicle, TPA/Vehicle and TPA/RM191A treated mice. The arrowheads indicate mast cells. Quantification of number of mast cells are shown in the right (n = 3). (D) NO production in ear tissue homogenates of acetone/Vehicle, TPA/Vehicle and TPA/RM191A treated mice (n = 4). (E) Representative images of wound areas on different days in RM191A (50 μL of 2.1 mg/mL) or Vehicle treated mice. The percentage wound closure is shown (n = 9). (F) Representative H&E staining images of wound areas in RM191A or Vehicle treated mice on Day 12. The arrowheads indicate the epidermal edges of the wound and white dotted lines indicate epidermal area (E: epidermis, D: dermis). The magnified view of the highlighted (black box) area is shown in the right. Quantification of epidermal gap, epidermal thickness and tissue granulation area are shown (n = 6). (G) Representative Masson's Trichrome staining images of dermal regions in regenerated skin from RM191A or Vehicle treated mice. Quantification of collagen (blue) content is shown (n = 8). (H) NO production in dorsal skin samples of mice (102-week-old) treated with RM191A or Vehicle for 7 days (n = 4). (I) Representative Toluidine blue stains of skin sections and mast cells numbers from mice (102-week-old) treated with RM191A or Vehicle for 7 days (n = 4).
Data expressed as mean ± SEM. *p < 0.05, **p < 0.005, ***p < 0.0005 and ****p < 0.00005 by *t*-test or One-way ANOVA. (For interpretation of the references to colour in this figure legend, the reader is referred to the Web version of this article.)

thickness and enhanced tissue granulation area of the skin areas of the RM191A-treated group when compared to the control group (Fig. 5F). Moreover, Masson's Trichrome staining revealed higher collagen deposition in the RM191A-treated dermal layer, compared to their control (Fig. 5G). Transition from the inflammatory phase to the proliferative phase is critical for proper wound healing, however, prolonged inflammation is detrimental and impedes keratinocyte activation and differentiation [55]. The levels of cytokines IL-1β, GRO-α, IL-6 and MCP-1 in the serum were downregulated by 85%, 66%, 90% and 70% respectively in RM191A-treated group on Day 12 compared to the control (Fig. S5A, S5B), indicating that systemic inflammation was suppressed by RM191A, thereby favoring the proliferative phase.

Finally, we tested if RM191A has any effects on skin aging. RM191A or Vehicle was topically applied to 102-week-old female mice for 7 consecutive days. Overall skin morphology as assessed using H&E staining was similar between the two groups (Fig. S5C). One of the hallmarks of skin aging is accumulation of ROS and RNS. When the NO concentration was determined in skin lysates, the RM191A-treated group exhibited lower NO levels compared to the control (Fig. 5H), implying a beneficial role of RM191A in reducing oxidative stress in aged skin. Next, we determined if RM191A affects mast cells in the dermis as it has been established that mast cells accumulate in the skin with increasing age and contribute to skin aging [56]. As shown in Fig. 5I, RM191A treatment significantly reduced the number of mast cells compared to the control. The combined results of these analyses led us to conclude that RM191A is effective in reducing the negative impacts of oxidative stress and inflammation in inflammatory-driven skin disorders, is regenerative of skin in wound healing, and is geroprotective when applied to skin.

4. Discussion

Native SODs are protective against various oxidative stress-mediated skin disorders. This fact has invoked interest in SOD mimetics for therapeutic applications. Among the various classes of SOD mimetics, only manganese porphyrin complexes have shown promise in clinical trials [57,58]. This is likely due to the fact that unlike previously reported iron and copper coordination complexes, manganese-based SOD mimetics have typically shown lower toxicity, higher activity and increased stability. RM191A is the next generation copper-based SOD mimetic that is highly stable and whose activity surpasses native SOD's abilities to scavenge free radicals and exceeds most of the manganese-based SOD-mimetics. There are several reasons for RM191A's high SOD-like activity. Each molecule of RM191A can react with three O_2^- ions while reducing Cu^{2+}-Cu^{3+} to Cu^{+}-Cu^{+}, whereas Mn^{2+}-based SOD-mimetics can react with one O_2^- ion (Fig. S2M). Moreover, the reduction potential indicates that the k_{cat} for Cu^{3+}/Cu^{2+} reduction is likely to be higher than that of Cu^{2+}/Cu^{+} reduction, although this entails further investigation. Furthermore, in cells RM191A upregulates various antioxidant genes, such as heme oxygenase, heat shock protein and thioredoxin reductase, and downregulates pro-inflammatory cytokines, including IL-1β, IL-6 and TNF-α, which can further boost its antioxidant capacity.

Despite its water solubility, RM191A was able to penetrate the skin and distribute into different internal organs via the bloodstream. Our toxicity results demonstrated that RM191A is well-tolerated in animals. A 26 g mouse can tolerate up to 50 μL of topical RM191A with no side effects. This is equivalent to 144 mL applied to the skin of a 75 kg human. We have further found that RM191A is stable in light and heat up to 30 °C for more than 12 months and that RM191A remains active and safe in a topical hydrogel formulation over this timeframe. As far as we are aware, all previous work identifying the biological activities of copper, including its molecular mechanisms, its role in oxidative stress, inflammation, immunomodulation, geroprotection and its homeostasis, specifically relate to Cu^{2+} as it would normally be present in the body [59–62]. As such, the biological activity of a Cu^{3+} containing coordination complex as is present in RM191A is reported here for the first time.

Topical RM191A shows promise as a photoprotective agent in human skin and was at least as active as 1,25D, generally acknowledged for its photoprotective properties [35,48–50,53]. One of the obvious reasons for this reduction in DNA damage is the scavenging of ROS and RNS by RM191A, although their levels were not directly tested in the human skin explants. This may even explain the lower CPD after 3 h, since ROS and RNS damage DNA repair enzymes and thus inhibit DNA repair [63–65]. Also, RM191A may reduce DNA damage by other mechanisms, such as increasing energy available for DNA repair, upregulating DNA repair enzymes or enhancing mitochondrial repair [35]. However, to verify this and other results it will be necessary to repeat this study in explants prepared from a range of donors with different skin types. Inadequately repaired DNA damage is a key factor leading to mutations and then to UV-induced skin tumours as well as photo-aging [48]. It would be worth testing whether RM191A application in a chronic UV-exposure model reduces skin tumours and/or photo-aging in the UV exposed areas.

The topical application of the RM191A demonstrated remarkable inhibition of inflammation in the TPA mouse ear model, which has significant implications for human use for the treatment of both acute and chronic inflammatory-driven diseases including skin conditions like psoriasis [66]. Similar to LPS, immune cell influx and subsequent ROS/RNS generation by TPA can activate the inflammatory cascade [67], which we have found is significantly inhibited by RM191A. The direct involvement of RM191A in downregulating inflammatory pathways was corroborated by gene expression analysis in RAW and NHDF, where RM191A inhibited the expression of many genes reported to be involved in skin inflammation. It is possible that the anti-inflammatory properties of RM191A are partly mediated by its ROS/RNS-scavenging activity. Although RM191A treatment demonstrated marked improvement in the healing rate of large, full-thickness excisional wounds in mice, the mechanism is not very clear to us as wound healing response is known to be orchestrated by retrograde inflammation and ROS

generation [68,69]. One of the possibilities is that RM191A facilitates the generation of new tissues (and collagen synthesis) by attenuating unwanted inflammation, as evident from the reduction in systemic inflammation in the late stage of wound healing, thereby accelerating the transition from inflammatory phase to proliferative phase. It will be interesting to investigate how RM191A performs in chronic non-healing wounds, diabetic ulcers, burns, limb damage and lacerations. Short-term application of RM191A reduced age-associated oxidative stress in skin, implying a geroprotective role of RM191A. In the next stage of our research we will be exploring the effects of long-term application of RM191A for the treatment of different age-related skin disorders.

One of the notable findings of our research was the significant, beneficial immunomodulation by RM191A, especially suppression of mast cells during skin inflammation and aging. Mast cells are innate immune cells resident in tissues, which store preformed inflammatory mediators in cytoplasmatic secretory granules which are released immediately after activation. Mast cells are the main cell type involved in allergic reactions, and are also associated with the adaptive immune response, including inflammatory and neurodegenerative diseases, traumatic brain injury, stroke, and stress disorders [70,71]. Mast cells are also becoming an important target for anti-aging therapy. RM191A is therefore likely to have a therapeutically beneficial effect on multiple diseases by targeting mast cell activity.

RM191A's ability to reduce oxidative stress, inflammation and modulate pain-associated biomarkers indicates that RM191A may have the potential to attenuate chronic pain. Although measurement of pain was beyond the scope of this study, RM191A is currently the subject of a Phase II human clinical trial for the treatment of neuropathic pain (HREC/16/HAWKE/483). In addition to demonstrating robust antioxidant and anti-inflammatory properties, RM191A might also facilitate the incorporation of copper into SOD1 and SOD3, ceruloplasmin and tissue repair enzymes - lysyl oxidase and elastase, which in turn can accelerate healing and inhibit inflammation. A similar mechanism has been proposed for Cu-ATSM, which is currently in clinical trial for motor neurone disease (MND) [72,73]. It may also be that RM191A is protective of mitochondria by eliminating ROS and RNS before they can cause oxidative damage, effectively preserving normal cell signalling and maintaining the integrity of the mitochondria.

Interestingly and perhaps importantly, it is now recognized that a "cytokine storm", predominantly driven by IL-1β, IL-6 and TNFα is a hallmark of the onset of severe COVID-19 symptoms. We have, in our work here, demonstrated that this same cytokine set is meaningfully reduced in the bloodstream by RM191A topical treatment. Finally, oxidative stress has been linked to a multitude of human diseases and conditions, including aging, bipolar disorder, cancer, chronic morphine intolerance, diabetes, eye diseases, fibromyalgia, ischemia, pain, radiation injury, reperfusion-related injuries – for example heart attack, stroke, and organ dysfunction; as well as neurodegenerative disorders like Alzheimer's, Parkinson's, MND, multiple sclerosis and epilepsy, to mention only a few [74]. RM191A's significant safety profile, its ability to neutralize ROS and RNS, simultaneously diminish or eliminate the inflammatory responses and easy bioavailability, sets it apart as a new therapeutic and means that it likely has significant benefit in the treatment of a wide variety of human diseases/conditions.

5. Conclusion

RM191A is a novel small molecule SOD mimetic that demonstrated significant SOD-like antioxidant and anti-inflammatory activities. These combined actions are likely the result of its unique, stable Cu^{2+}/Cu^{3+} dimers. RM191A exhibited protective effects towards a wide range of cells against oxidative stress by suppressing ROS and RNS levels and via modulating the expression of several key genes associated with oxidative stress and inflammation. The topical application of RM191A beneficially and significantly reduced three types of UV-induced DNA damage in human skin explants in the epidermis and in the dermis. This reduction in DNA damage was similar to that produced by a well-established photoprotective agent, 1,25D. RM191A easily penetrated the skin layers and was readily distributed systemically throughout the body in mice. Both short-term and long-term dosing of RM191A did not exhibit any adverse effects in mice. It's topical application significantly reduced TPA-induced ear inflammation, accelerated excisional wound repair and diminished skin aging in mice. In conclusion, RM191A represents a new class of SOD mimetic which through its prodigious ROS/RNS sequestering, anti-inflammatory activity, and immunomodulation exhibits beneficial effects in various skin disorders.

Declaration of competing interest

LC is the Director and co-founder of RR MedSciences that holds patents for the synthesis and application of RM191A. Research studies at Macquarie University, University of New South Wales and University of Sydney were funded by RR MedSciences.

Acknowledgements

This paper is dedicated to our co-author Alistair J. Laos, a brilliant young mind and a promising scientist, whom we lost too soon. The mouse experiments were supported by NSW-Government Tech Voucher Grant (RG183345) awarded to RR MedSciences and AD. We would like to acknowledge staff at Macquarie University, University of Sydney, UNSW Mark Wainwright Analytical Centre Facilities (EMU, SSEAU, Flow Cytometry, BRIL, NMR), UNSW BRC, and especially Fei Shang (UNSW BMIF) and Tim Patton (Crux Biolabs) for their support during the study.

Appendix A. Supplementary data

Supplementary data to this article can be found online at https://doi.org/10.1016/j.redox.2020.101790.

References

[1] J. D'Orazio, S. Jarrett, A. Amaro-Ortiz, T. Scott, UV radiation and the skin, Int. J. Mol. Sci. 14 (2013) 12222–12248.
[2] L.M. Hollestein, T. Nijsten, An insight into the global burden of skin diseases, J. Invest. Dermatol. 134 (2014) 1499–1501.
[3] M.K. Basra, M. Shahrukh, Burden of skin diseases, Expert Rev. Pharmacoecon. Outcomes Res. 9 (2009) 271–283.
[4] F.A.S. Addor, Beyond photoaging: additional factors involved in the process of skin aging, Clin. Cosmet. Invest. Dermatol. 11 (2018) 437–443.
[5] M. Rinnerthaler, J. Bischof, M.K. Streubel, A. Trost, K. Richter, Oxidative stress in aging human skin, Biomolecules 5 (2015) 545–589.
[6] D.R. Bickers, M. Athar, Oxidative stress in the pathogenesis of skin disease, J. Invest. Dermatol. 126 (2006) 2565–2575.
[7] T. Finkel, N.J. Holbrook, Oxidants, oxidative stress and the biology of ageing, Nature 408 (2000) 239–247.
[8] M. Schieber, N.S. Chandel, ROS function in redox signaling and oxidative stress, Curr. Biol. 24 (2014) R453–R462.
[9] S. Di Meo, T.T. Reed, P. Venditti, V.M. Victor, Role of ROS and RNS sources in physiological and pathological conditions, Oxid Med Cell Longev (2016) 1245049, 2016.
[10] F.A.S. Addor, Antioxidants in dermatology, An. Bras. Dermatol. 92 (2017) 356–362.
[11] S. Reuter, S.C. Gupta, M.M. Chaturvedi, B.B. Aggarwal, Oxidative stress, inflammation, and cancer: how are they linked? Free Radic. Biol. Med. 49 (2010) 1603–1616.
[12] L. Alvarez-Arellano, N. Gonzalez-Garcia, M. Salazar-Garcia, J.C. Corona, Antioxidants as a potential target against inflammation and oxidative stress in attention-deficit/hyperactivity disorder, Antioxidants **9** (2020).
[13] S.K. Biswas, Does the interdependence between oxidative stress and inflammation explain the antioxidant paradox? Oxid Med Cell Longev (2016) 5698931, 2016.
[14] J. Hakim, [Reactive oxygen species and inflammation], C. R. Seances Soc. Biol. Fil. 187 (1993) 286–295.
[15] I. Fridovich, Superoxide dismutases, Annu. Rev. Biochem. 44 (1975) 147–159.
[16] L. Chen, J.Y. Hu, S.Q. Wang, The role of antioxidants in photoprotection: a critical review, J. Am. Acad. Dermatol. 67 (2012) 1013–1024.
[17] S. Le Quéré, D. Lacan, B. Lemaire, J. Carillon, K. Schmitt, The role of superoxide dismutase (SOD) in skin disorders, Nutrafoods 13 (2014) 13–27.
[18] Y. Iuchi, D. Roy, F. Okada, N. Kibe, S. Tsunoda, S. Suzuki, M. Takahashi, H. Yokoyama, J. Yoshitake, S. Kondo, J. Fujii, Spontaneous skin damage and

delayed wound healing in SOD1-deficient mice, Mol. Cell. Biochem. 341 (2010) 181–194.
[19] K. Yasui, A. Baba, Therapeutic potential of superoxide dismutase (SOD) for resolution of inflammation, Inflamm. Res. 55 (2006) 359–363.
[20] J.M. McCord, M.A. Edeas, SOD, oxidative stress and human pathologies: a brief history and a future vision, Biomed. Pharmacother. 59 (2005) 139–142.
[21] J.J. Perry, D.S. Shin, E.D. Getzoff, J.A. Tainer, The structural biochemistry of the superoxide dismutases, Biochim. Biophys. Acta 1804 (2010) 245–262.
[22] P.J. Hart, M.M. Balbirnie, N.L. Ogihara, A.M. Nersissian, M.S. Weiss, J.S. Valentine, D. Eisenberg, A structure-based mechanism for copper-zinc superoxide dismutase, Biochemistry 38 (1999) 2167–2178.
[23] J.A. Tainer, E.D. Getzoff, J.S. Richardson, D.C. Richardson, Structure and mechanism of copper, zinc superoxide dismutase, Nature 306 (1983) 284–287.
[24] K.G.S. Lippard, S.J. a, Chemistry of the imidazolate-bridged bimetallic center in the Cu-Zn superoxide dismutase and its model compounds, Accounts Chem. Res. 15 (1982) 318–326.
[25] D. Salvemini, D.P. Riley, S. Cuzzocrea, SOD mimetics are coming of age, Nat. Rev. Drug Discov. 1 (2002) 367–374.
[26] K. Stover, T. Fukuyama, A.T. Young, M.A. Daniele, R. Oberley, J.D. Crapo, W. Baumer, Topically applied manganese-porphyrins BMX-001 and BMX-010 display a significant anti-inflammatory response in a mouse model of allergic dermatitis, Arch. Dermatol. Res. 308 (2016) 711–721.
[27] R. Bonetta, Potential therapeutic applications of MnSODs and SOD-mimetics, Chemistry 24 (2018) 5032–5041.
[28] T. Fujiwara, D. Duscher, K.C. Rustad, R. Kosaraju, M. Rodrigues, A.J. Whittam, M. Januszyk, Z.N. Maan, G.C. Gurtner, Extracellular superoxide dismutase deficiency impairs wound healing in advanced age by reducing neovascularization and fibroblast function, Exp. Dermatol. 25 (2016) 206–211.
[29] R. Novotna, Z. Travnicek, R. Herchel, SOD-mimic Cu(II) dimeric complexes involving kinetin and its derivative: preparation and characterization, Bioinorgan. Chem. Appl. (2012) 704329, 2012.
[30] M. Liakopoulou-Kyriakides, S. Hadjispyrou, A. Zarkadis, Cu(III)-polypeptide complexes exhibiting SOD-like activity, Amino Acids 16 (1999) 415–423.
[31] C. Beauchamp, I. Fridovich, Superoxide dismutase: improved assays and an assay applicable to acrylamide gels, Anal. Biochem. 44 (1971) 276–287.
[32] A. Das, G.X. Huang, M.S. Bonkowski, A. Longchamp, C. Li, M.B. Schultz, L.J. Kim, B. Osborne, S. Joshi, Y. Lu, J.H. Trevino-Villarreal, M.J. Kang, T.T. Hung, B. Lee, E. O. Williams, M. Igarashi, J.R. Mitchell, L.E. Wu, N. Turner, Z. Arany, L. Guarente, D.A. Sinclair, Impairment of an endothelial NAD(+)-H2S signaling network is a reversible cause of vascular aging, Cell 173 (2018) 74–89 e20.
[33] S. Sekhar, K.K. Sampath-Kumara, S.R. Niranjana, H.S. Prakash, Attenuation of reactive oxygen/nitrogen species with suppression of inducible nitric oxide synthase expression in RAW 264.7 macrophages by bark extract of Buchanania lanzan, Phcog. Mag. 11 (2015) 283–291.
[34] E.J. Song, C. Gordon-Thomson, L. Cole, H. Stern, G.M. Halliday, D.L. Damian, V. E. Reeve, R.S. Mason, 1alpha,25-Dihydroxyvitamin D3 reduces several types of UV-induced DNA damage and contributes to photoprotection, J. Steroid Biochem. Mol. Biol. 136 (2013) 131–138.
[35] M.S. Rybchyn, W.G.M. De Silva, V.B. Sequeira, B.Y. McCarthy, A.V. Dilley, K. M. Dixon, G.M. Halliday, R.S. Mason, Enhanced repair of UV-induced DNA damage by 1,25-dihydroxyvitamin D3 in skin is linked to pathways that control cellular energy, J. Invest. Dermatol. 138 (2018) 1146–1156.
[36] N. Mersmann, D. Tkachev, R. Jelinek, P.T. Roth, W. Mobius, T. Ruhwedel, S. Ruhle, W. Weber-Fahr, A. Sartorius, M. Klugmann, Aspartoacylase-lacZ knockin mice: an engineered model of Canavan disease, PloS One 6 (2011), e20336.
[37] A.S. Aguiar Jr., E.L. Moreira, A.A. Hoeller, P.A. Oliveira, F.M. Cordova, V. Glaser, R. Walz, R.A. Cunha, R.B. Leal, A. Latini, R.D. Prediger, Exercise attenuates levodopa-induced dyskinesia in 6-hydroxydopamine-lesioned mice, Neuroscience 243 (2013) 46–53.
[38] H. Inoue, T. Mori, S. Shibata, Y. Koshihara, Modulation by glycyrrhetinic acid derivatives of TPA-induced mouse ear oedema, Br. J. Pharmacol. 96 (1989) 204–210.
[39] J. Succar, G. Giatsidis, N. Yu, K. Hassan, R. Khouri Jr., M.F. Gurish, G. Pejler, M. Abrink, D.P. Orgill, Mouse mast cell protease-4 recruits leukocytes in the inflammatory phase of surgically wounded skin, Adv. Wound Care 8 (2019) 469–475.
[40] T. Offer, A. Russo, A. Samuni, The pro-oxidative activity of SOD and nitroxide SOD mimics, Faseb. J. 14 (2000) 1215–1223.
[41] S. Holmes, B. Abbassi, C. Su, M. Singh, R.L. Cunningham, Oxidative stress defines the neuroprotective or neurotoxic properties of androgens in immortalized female rat dopaminergic neuronal cells, Endocrinology 154 (2013) 4281–4292.
[42] H.Y. Hsu, M.H. Wen, Lipopolysaccharide-mediated reactive oxygen species and signal transduction in the regulation of interleukin-1 gene expression, J. Biol. Chem. 277 (2002) 22131–22139.
[43] J.A. Lee, H.Y. Song, S.M. Ju, S.J. Lee, H.J. Kwon, W.S. Eum, S.H. Jang, S.Y. Choi, J. S. Park, Differential regulation of inducible nitric oxide synthase and cyclooxygenase-2 expression by superoxide dismutase in lipopolysaccharide stimulated RAW 264.7 cells, Exp. Mol. Med. 41 (2009) 629–637.
[44] P.J. Ferret, E. Soum, O. Negre, D. Fradelizi, Auto-protective redox buffering systems in stimulated macrophages, BMC Immunol. 3 (2002) 3.
[45] P. Pelegrin, C. Barroso-Gutierrez, A. Surprenant, P2X7 receptor differentially couples to distinct release pathways for IL-1beta in mouse macrophage, J. Immunol. 180 (2008) 7147–7157.
[46] R.R. Ji, A. Chamessian, Y.Q. Zhang, Pain regulation by non-neuronal cells and inflammation, Science 354 (2016) 572–577.
[47] S. Dunaway, R. Odin, L. Zhou, L. Ji, Y. Zhang, A.L. Kadekaro, Natural antioxidants: multiple mechanisms to protect skin from solar radiation, Front. Pharmacol. 9 (2018) 392.
[48] R.S. Mason, J. Reichrath, Sunlight vitamin D and skin cancer, Anticancer Agents Med Chem 13 (2013) 83–97.
[49] R. Gupta, K.M. Dixon, S.S. Deo, C.J. Holliday, M. Slater, G.M. Halliday, V.E. Reeve, R.S. Mason, Photoprotection by 1,25 dihydroxyvitamin D3 is associated with an increase in p53 and a decrease in nitric oxide products, J. Invest. Dermatol. 127 (2007) 707–715.
[50] K.M. Dixon, A.W. Norman, V.B. Sequeira, R. Mohan, M.S. Rybchyn, V.E. Reeve, G. M. Halliday, R.S. Mason, 1alpha,25(OH)(2)-vitamin D and a nongenomic vitamin D analogue inhibit ultraviolet radiation-induced skin carcinogenesis, Canc. Prev. Res. 4 (2011) 1485–1494.
[51] I.L. Steffensen, H. Dirven, S. Couderq, A. David, S.C. D'Cruz, M.F. Fernandez, V. Mustieles, A. Rodriguez-Carrillo, T. Hofer, Bisphenols and oxidative stress biomarkers-associations found in human studies, evaluation of methods used, and strengths and weaknesses of the biomarkers, Int. J. Environ. Res. Publ. Health **17** (2020).
[52] L.R. Walker, M. Rattigan, J. Canterino, A case of isolated elevated copper levels during pregnancy, J. Pregnancy (2011) 385767, 2011.
[53] H.Y. Song, J.A. Lee, S.M. Ju, K.Y. Yoo, M.H. Won, H.J. Kwon, W.S. Eum, S.H. Jang, S.Y. Choi, J. Park, Topical transduction of superoxide dismutase mediated by HIV-1 Tat protein transduction domain ameliorates 12-O-tetradecanoylphorbol-13-acetate (TPA)-induced inflammation in mice, Biochem. Pharmacol. 75 (2008) 1348–1357.
[54] T.S. Rao, J.L. Currie, A.F. Shaffer, P.C. Isakson, Comparative evaluation of arachidonic acid (AA)- and tetradecanoylphorbol acetate (TPA)-induced dermal inflammation, Inflammation 17 (1993) 723–741.
[55] C.K. Sen, G.M. Gordillo, S. Roy, R. Kirsner, L. Lambert, T.K. Hunt, F. Gottrup, G. C. Gurtner, M.T. Longaker, Human skin wounds: a major and snowballing threat to public health and the economy, Wound Repair Regen. 17 (2009) 763–771.
[56] S.M. Pilkington, M.J. Barron, R.E.B. Watson, C.E.M. Griffiths, S. Bulfone-Paus, Aged human skin accumulates mast cells with altered functionality that localize to macrophages and vasoactive intestinal peptide-positive nerve fibres, Br. J. Dermatol. 180 (2019) 849–858.
[57] I. Batinic-Haberle, M.E. Tome, Thiol regulation by Mn porphyrins, commonly known as SOD mimics, Redox Biol 25 (2019) 101139.
[58] Y. Yulyana, A. Tovmasyan, I.A. Ho, K.C. Sia, J.P. Newman, W.H. Ng, C.M. Guo, K. M. Hui, I. Batinic-Haberle, P.Y. Lam, Redox-active Mn porphyrin-based potent SOD mimic, MnTnBuOE-2-PyP(5+), enhances carbenoxolone-mediated TRAIL-induced apoptosis in Glioblastoma multiforme, Stem Cell Rev Rep 12 (2016) 140–155.
[59] M. Arredondo, M.T. Nunez, Iron and copper metabolism, Mol. Aspect. Med. 26 (2005) 313–327.
[60] K.G. Daniel, P. Gupta, R.H. Harbach, W.C. Guida, Q.P. Dou, Organic copper complexes as a new class of proteasome inhibitors and apoptosis inducers in human cancer cells, Biochem. Pharmacol. 67 (2004) 1139–1151.
[61] S. Puig, D.J. Thiele, Molecular mechanisms of copper uptake and distribution, Curr. Opin. Chem. Biol. 6 (2002) 171–180.
[62] J.Y. Uriu-Adams, C.L. Keen, Copper, oxidative stress, and human health, Mol. Aspect. Med. 26 (2005) 268–298.
[63] M. Jaiswal, N.F. LaRusso, L.J. Burgart, G.J. Gores, Inflammatory cytokines induce DNA damage and inhibit DNA repair in cholangiocarcinoma cells by a nitric oxide-dependent mechanism, Canc. Res. 60 (2000) 184–190.
[64] T. Nguyen, D. Brunson, C.L. Crespi, B.W. Penman, J.S. Wishnok, S.R. Tannenbaum, DNA damage and mutation in human cells exposed to nitric oxide in vitro, Proc. Natl. Acad. Sci. U. S. A. 89 (1992) 3030–3034.
[65] D.T.G.J.R. Bau, K.Y. Jan, Nitric oxide is involved in arsenite inhibition of pyrimidine dimer excision, Carcinogenesis 22 (2001) 709–716.
[66] M.P. Schon, W.H. Boehncke, Psoriasis, N. Engl. J. Med. 352 (2005) 1899–1912.
[67] R. Huang, L. Zhao, H. Chen, R.H. Yin, C.Y. Li, Y.Q. Zhan, J.H. Zhang, C.H. Ge, M. Yu, X.M. Yang, Megakaryocytic differentiation of K562 cells induced by PMA reduced the activity of respiratory chain complex IV, PloS One 9 (2014), e96246.
[68] T.J. Koh, L.A. DiPietro, Inflammation and wound healing: the role of the macrophage, Expet Rev. Mol. Med. 13 (2011) e23.
[69] C. Dunnill, T. Patton, J. Brennan, J. Barrett, M. Dryden, J. Cooke, D. Leaper, N. T. Georgopoulos, Reactive oxygen species (ROS) and wound healing: the functional role of ROS and emerging ROS-modulating technologies for augmentation of the healing process, Int. Wound J. 14 (2017) 89–96.
[70] D. Kempuraj, G.P. Selvakumar, M.E. Ahmed, S.P. Raikwar, R. Thangavel, A. Khan, S.A. Zaheer, S.S. Iyer, C. Burton, D. James, A. Zaheer, COVID-19, mast cells, cytokine storm, psychological stress, and neuroinflammation 1073858420941476, Neuroscientist, 2020.
[71] A. Troupin, D. Shirley, B. Londono-Renteria, A.M. Watson, C. McHale, A. Hall, A. Hartstone-Rose, W.B. Klimstra, G. Gomez, T.M. Colpitts, A role for human skin mast cells in dengue virus infection and systemic spread, J. Immunol. 197 (2016) 4382–4391.

[72] https://www.mndaust.asn.au/Discover-our-research/Latest-research/Clinical-trials/Copper-ATSM-Clinical-Trial.aspx.
[73] B.R. Roberts, N.K. Lim, E.J. McAllum, P.S. Donnelly, D.J. Hare, P.A. Doble, B. J. Turner, K.A. Price, S.C. Lim, B.M. Paterson, J.L. Hickey, T.W. Rhoads, J. R. Williams, K.M. Kanninen, L.W. Hung, J.R. Liddell, A. Grubman, J.F. Monty, R. M. Llanos, D.R. Kramer, J.F. Mercer, A.I. Bush, C.L. Masters, J.A. Duce, Q.X. Li, J. S. Beckman, K.J. Barnham, A.R. White, P.J. Crouch, Oral treatment with Cu(II) (atsm) increases mutant SOD1 in vivo but protects motor neurons and improves the phenotype of a transgenic mouse model of amyotrophic lateral sclerosis, J. Neurosci. 34 (2014) 8021–8031.
[74] I. Batinic-Haberle, J.S. Reboucas, I. Spasojevic, Superoxide dismutase mimics: chemistry, pharmacology, and therapeutic potential, Antioxidants Redox Signal. 13 (2010) 877–918.